Available online at www.sciencedirect.com
ScienceDirect
Journal of Photochemistry and Photobiology A: Chemistry 184 (2006) 1–17
Journal of Photochemistry and Photobiology A:Chemistry
www.elsevier.com/locate/jphotochem

The photophysics of cryptophyte light-harvesting

Alexander B. Doust [a], Krystyna E. Wilk [b], Paul M.G. Curmi [b], Gregory D. Scholes [a,*]

[a] *Lash Miller Chemical Laboratory, 80 St. George Street, Institute for Optical Sciences, Centre for Quantum Information and Quantum Control, University of Toronto, Toronto, Ontario M5S 3H6, Canada*

[b] *School of Physics and Centre for Immunology, The University of New South Wales, Sydney, NSW 2052, Australia*

Received 20 March 2006; received in revised form 13 June 2006; accepted 14 June 2006
Available online 24 July 2006

Abstract

Recent studies of the optical properties and the critical role of phycobiliproteins in the absorption of green light for photosynthesis in cryptophyte algae (*Rhodomonas CS24* and *Chroomonas CCMP270*) are reviewed. Investigations of two different isolated proteins, phycoerythrin 545 (PE545) and phycocyanin 645 (PC645), whose crystal structures are known to 0.97 and 1.4 Å resolution respectively, are described. Steady-state spectroscopic measurements, including polarization anisotropy and circular dichroism, are used in combination with ultrafast transient grating and transient absorption techniques to elucidate a detailed picture of resonance energy transfer within the light-harvesting proteins. Quantum chemical calculations are employed to estimate phycobilin excited states, and generate transition density cubes which are used to calculate accurately the electronic coupling between the chromophores in PE545 and PC645. Energy transfer dynamics are examined using the generalized Förster theory. Kinetic models for energy transfer dynamics in both proteins are presented for comparison. Investigations of energy transfer from phycoerythrin 545 to chlorophyll-containing light harvesting complexes and photosystems in the intact algae *Rhodomonas CS24* and *Chroomonas CCMP270* are also reported.

Keywords: Cryptophytes; Photosynthesis; Energy transfer; Spectroscopy; Phycobiliproteins

1. Cryptophytes and photosynthesis

Cyanobacteria are widely credited with the introduction of oxygen evolving photosynthesis into the biosphere at least 3 billion years ago by learning to tap into a freely available resource—the hydrogen that exists in spectacular abundance in water [1–4]. Photosynthesis is now an important part of life on earth. We owe the oxygen we breathe, the carbon fossil fuels we burn and almost all of the food we eat to the transformation of sunlight into chemical energy [5,6].

Cryptophytes (genus Cryptomonas) are single celled photosynthetic algae, 6–20 μm in size, and abundant in both fresh- and seawater, where they live at the bottom of shallow water and can survive in low light conditions [7,8]. They are an evolutionary oddity, emerging as a unique lineage from cyanobacterial red algae after a secondary endosymbiosis event, in which a remnant of the red algal nucleus, the nucleomorph, was retained [9]. As a result, the engulfed red algal cell is enclosed in the membrane and the light-harvesting (LH) system is based on proteins homologous to red algal phycobiliproteins (PBPs). During the course of evolution, the phycobilisomes of the red algae were reduced and allophycocyanin disappeared. The aggregation state of the biliproteins changed from a trimeric to a heterodimeric structure. In addition, the remaining phycoerythrin or phycocyanin was transferred into the luminal space of the thylakoid membrane. This is the most striking difference between cryptophyte biliproteins and those in other algae; instead of being present as phyobilisomes on the stromal surface of the thylakoid membrane, the cryptophyte biliproteins occur as a dense granular matrix filling the interior of the thylakoid [10].

In the aquatic environments inhabited by cryptophytes, the available spectral window and quantity of light is reduced. Water absorption in part defines the visible spectrum available (Fig. 1), potentially attenuating enough red light to leave reaction centers (RC) in the dark. Chlorophyll (Chl) and carotenoid (Car) absorption is minimal in the 450–640 nm region. To compensate for that, cryptophyte photosynthesis utilizes phycobiliproteins as the primary LH antennae to ensure photon capture across a wide range of wavelengths, typically optimized for the blue and green spectral region.

* Corresponding author. Tel.: +1 416 946 7532; fax: +1 416 978 8775.
E-mail address: gscholes@chem.utoronto.ca (G.D. Scholes).

1010-6030/$ – see front matter © 2006 Elsevier B.V. All rights reserved.
doi:10.1016/j.jphotochem.2006.06.006

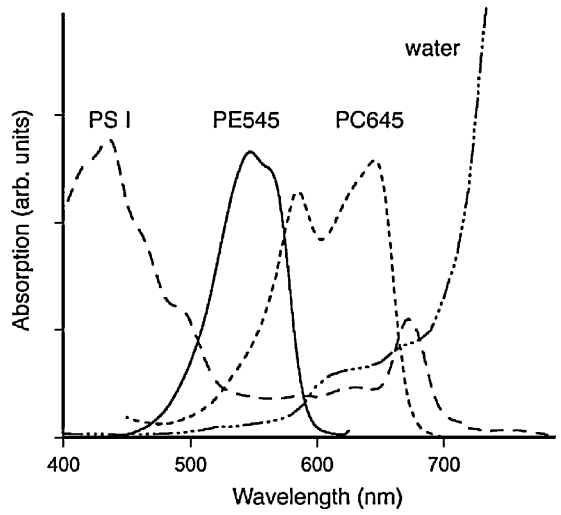

Fig. 1. The availability of light for aquatic photosynthetic organisms is determined in part by water absorption. Phycobiliproteins, PC645 (short-dashed) and PE545 (solid), absorbs in the region where water absorption (dash-dotted) and Chl and Car absorption (PS I, long-dashed) is minimal. The absorption coefficients are arbitrary with the absorption maxima of the three photosynthetic proteins shown to be equal.

Owing to the lumenal location of the cryptophyte biliproteins, the mechanism of light harvesting is expected to be significantly different from that known for the phycobilisomes of cyanobacteria and red algae [11]. Cryptophytes are the sole organism that have the unique pigment combination of Chl *a*, Chl *c2*, the carotenoid alloxanthin in addition to one of two phycobiliproteins, phycoerythrin or phycocyanin [12,13]. These phycobiliproteins contain open-chain tetrapyrrole pigments covalently bound to the apoprotein. Tuning of the spectroscopic properties is achieved through complex noncovalent interactions and as well as chromophore–chromophore (electronic) interactions [10,14–16]. There are good reasons for strong excitonic interactions between bilins in such proteins. For example, they increase the spectral range of absorption by splitting the energy levels of degenerate bilins into high- and low-energy bands. Fast internal conversion subsequently traps the excitation on the low-energy excitonic state [17–22]. Protonation of the bilin chromophores by aspartate residues close to the two central nitrogens is an additional source for increased spectra coverage [23,24]. The resulting spectroscopic diversity allows these phycobiliproteins to cover >3500 cm^{-1} of the visible spectrum between the Soret and Q_y bands of Chl *a* using only two or three chemically distinct bilin chromophores [10,25].

The structures of two cryptophyte biliproteins, phycoerythrin 545 (PE545) and phycocyanin 645 (PC645), are now known, and it is of interest to elucidate the operation of light harvesting and energy transfer in these proteins as well as the transfer of excitation from these peripheral antenna proteins to the reaction center chlorophylls. This review summarizes the results of investigations of *Rhodomonas CS24* (formerly *Chroomonas CS24*), from which PE545 is isolated, and *Chroomonas CCMP270*, from which PC645 is isolated. The former has been obtained from CSIRO, the Department of Fisheries in Hobart, and the latter from the Provasoli-Guillard National Center for Culture of Marine Phytoplankton (CCMP), Bigelow Laboratory for Ocean Sciences, both in Australia.

1.1. Energy transfer and photosynthetic architecture in cryptophytes

Resonance energy transfer is a photophysical process that causes migration of excitation energy among chromophores over distances typically in the range 0.5–10 nm. A photoexcited donor molecule transfers its electronic excitation energy to an acceptor by means of a correlated mechanism that diminishes the lifetime of the donor and can be thought of as a virtual photon exchange between donor and acceptor that has been facilitated by an electronic coupling *V*. Many of the light-harvesting processes in photosynthesis have been understood on the basis of Förster's theory, which makes the association between the rate of energy transfer, *k*, and the electronic spectra of donor and acceptor molecules [26,27]. It is often written in terms of τ_D, the excited state lifetime of the donor, and R_0, the Förster critical distance, to highlight the R^{-6} dependence of the energy transfer rate. *R* is the center-to-center separation between donor and acceptor

$$k = \frac{1}{\tau_D}\left(\frac{R_0}{R}\right)^6 \tag{1a}$$

$$= \frac{2\pi}{\hbar}|V|^2 J \tag{1b}$$

Alternatively, the Fermi golden rule expression can be written explicitly, Eq. (1b), to show how *k* depends on the electronic interaction between their transition moments $V \propto V_{dip–dip}$ and a spectral overlap term, *J* [28–33].

Förster theory assumes the electronic coupling can be approximated as a dipole–dipole interaction ($V_{dip–dip} \propto 1/R^3$) [34–40]. The emission lifetime and line shape, absorption line shape, and oscillator strength are assumed to be unperturbed by the electronic interaction, static disorder is absent, and the energy transfer dynamics are incoherent. Owing to approximations inherent in the Fermi golden rule, the theory holds in the limit of very weak electronic coupling between donor and acceptor. In instances where the electronic coupling is not weak, such as among the B850 chromophores in LH2, energy transfer has been described using more sophisticated theories, including modified Redfield theory [41–45] and multichromophore Forster resonance energy transfer [46]. The beauty of a Förster-type formulation, however, is that the theory tends to provide clearer physical insights. That idea motivated the development of generalized Förster theory [20,21,32,33,47] which allows many problems to be reformulated into a weakly coupled effective donor and effective acceptor representation.

A central ingredient of any theory for electronic energy transfer is the donor–acceptor electronic coupling, *V*. When the center-to-center distance *R* is comparable to the size of the molecules involved, then $V_{dip–dip}$ may not be an accurate representation of *V* because information regarding the shape of the interacting molecules is discarded when the dipole approximation is invoked [32,33,40,47]. In particular, molecules with

extended or asymmetric transition densities tend to exaggerate errors in the dipole–dipole approximation. In this case, information on transitions of each molecule should be retained as a transition density, rather than a dipole transition moment. Then the Coulombic coupling may be expressed quite accurately as the interaction between the transition densities connecting the ground and excited state of the donor and acceptor, $P^{D}(\mathbf{r}_1)$ and $P^{A}(\mathbf{r}_2)$ [32,33]:

$$V = \int d\mathbf{r}_1\, d\mathbf{r}_2 \frac{P^{D}(\mathbf{r}_1)P^{A}(\mathbf{r}_2)}{4\pi\varepsilon_0 \mathbf{r}_{12}} \quad (2)$$

where $\mathbf{r}_{12} = \mathbf{r}_1 - \mathbf{r}_2$. Below we describe how to calculate such electronic couplings and report results for PE545. To account more accurately for electronic coupling using a Förster-type expression it is convenient to introduce a generalized Förster critical transfer distance R_G to replace the standard R_0. We define [40]

$$R_G = \eta R_0 \quad (3)$$

where the correction factor $\eta = (V/V_{dip-dip})^{1/3}$ accounts for deviations from the dipole approximation.

To ensure an energy trapping efficiency above 90% in photosynthesis, the excitation should reach the reaction center within 1/10 of the excited state lifetime, that is, in a few hundred picoseconds. The quantum efficiency Q of one energy transfer step is estimated from the energy transfer rate k and the fluorescence lifetime of the donor in the absence of the acceptor, $\tau_D = 1/k_D$, by

$$Q = \frac{k}{k + k_D} \quad (4)$$

The three main chlorophyll–protein complexes that have been isolated from the thylakoid membranes of the cryptophyte *Rhodomonas CS24* are photosystem I (PS I), photosystem II (PS II), and a Chl *a*/*c2* carotenoid light harvesting complex (LHC) [48,49,50]. The LHC belongs to the same family of proteins as those of higher plants and *Rhodophyceae* [50,51] and accounts for 45% of the total Chl *a* and most of the Chl *c2* and xanthophylls. It has been shown to exhibit very efficient energy transfer from Chl *c2* to Chl *a* [50]. The thylakoids of *Rhodomonas* show some stacking and segregation of PS I and PS II, as in higher plants, but have a wider lumenal space [52–55]. A model of the organization of proteins in the thylakoid membrane [48] of cryptophyte algae is shown in Fig. 2. PS I is most likely limited to the unstacked regions, whereas the Chl *a*/*c2* LHC may be predominantly located in the stacked regions of the thylakoids [10,56]. PE545 is densely packed in the thylakoid lumen and displays no preferential orientation, neither relative to each other nor to the membrane [51].

The energy transfer pathways for phycobiliprotein excitations to the photosystems are poorly understood. Bruce et al. [13] recorded an increased contribution of phycobiliproteins to the excitation spectrum of PS II with respect to PS I in several cryptophyte algae and thus proposed preferred energy transfer from the phycobiliproteins to PS II over PS I. The same paper covers time-resolved fluorescence emission measurements at 77 K on

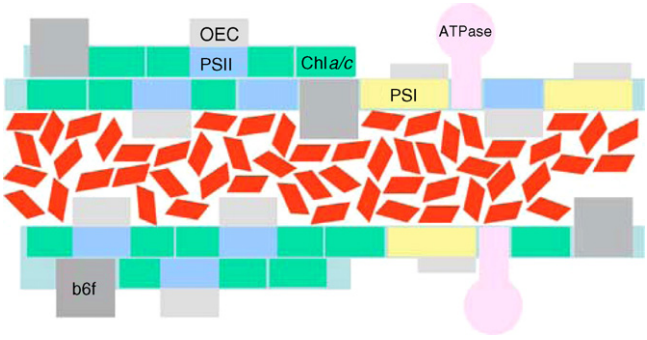

Fig. 2. A model of the cryptophyte thylakoid membrane adapted from Ref. [48]. The Chl *a*/*c2* antenna (dark green) can be found both in the grana and stroma of the thylakoid membrane. The PS II core complex (blue) is largely confined to the stacked regions of the membrane of which two grana stacks are displayed on the left. The stromal part of the membrane is shown at the right, and hosts the PS I complex (yellow). PE545 (red) is densely packed inside the lumen. The non-chlorophyll-containing components, including the extrinsic parts of the PS II core complex involved in water oxidation, are in grey. The distance between PE545 and the chlorophylls of PS I and the Chl *a*/*c2* antenna may be short, while that between PE545 and the chlorophylls of the PS II core can be much larger because of the presence of extrinsic proteins.

C. Salina, revealing a fluorescence decay time of 110 ps, for both phycobiliprotein and Chl *c2* fluorescence. It is thus suggested that energy transfer from phycobiliproteins to Chl *a* in the membrane is mediated by Chl *c2*, where the first step is rate limiting. Lichtlé et al. measured 77 K fluorescence excitation spectra of PS I and PS II, both under low and high light conditions [57]. In this way, they show that spillover from PS II to PS I under high light is solely mediated by the Chl antenna of PS II and does not involve phycobiliproteins. Consequently, they suggested that the PS II antenna is composed of both phycobiliproteins and Chls, whereas PS I is provided with energy by Chls only [14]. This model strongly resembles that proposed by Mimuro et al. [58], wherein the excitation energy from PE545 is transferred to the Chl *a*/*c2* light harvesting complex which is bound to PS II.

2. Phycoerythrin 545

2.1. Structure

The crystal structure of PE545 has been determined at an ultrahigh resolution of up to 0.97 Å [59,60]. The structural model is shown in Fig. 3 together with the chemical structures of the bound light-absorbing bilin molecules. In Fig. 4 the arrangement of the bilin molecules is shown through the protein scaffold. At ~60 kDa, and dimension of 75 Å × 60 Å × 45 Å, this is currently the largest protein structure known at atomic resolution. PE545 consists of four polypeptide chains, α_1, α_2 plus two β subunits, arranged in a complex known by convention as a dimer of αβ monomers. This complex is unique to the cryptophyte PBPs and it is unusual in that it contains a deep, water-filled slot between the monomers.

Each β subunit is covalently linked to three phycoerythrobilin (PEB) chromophores, labeled β82, β158 and β50/β61,

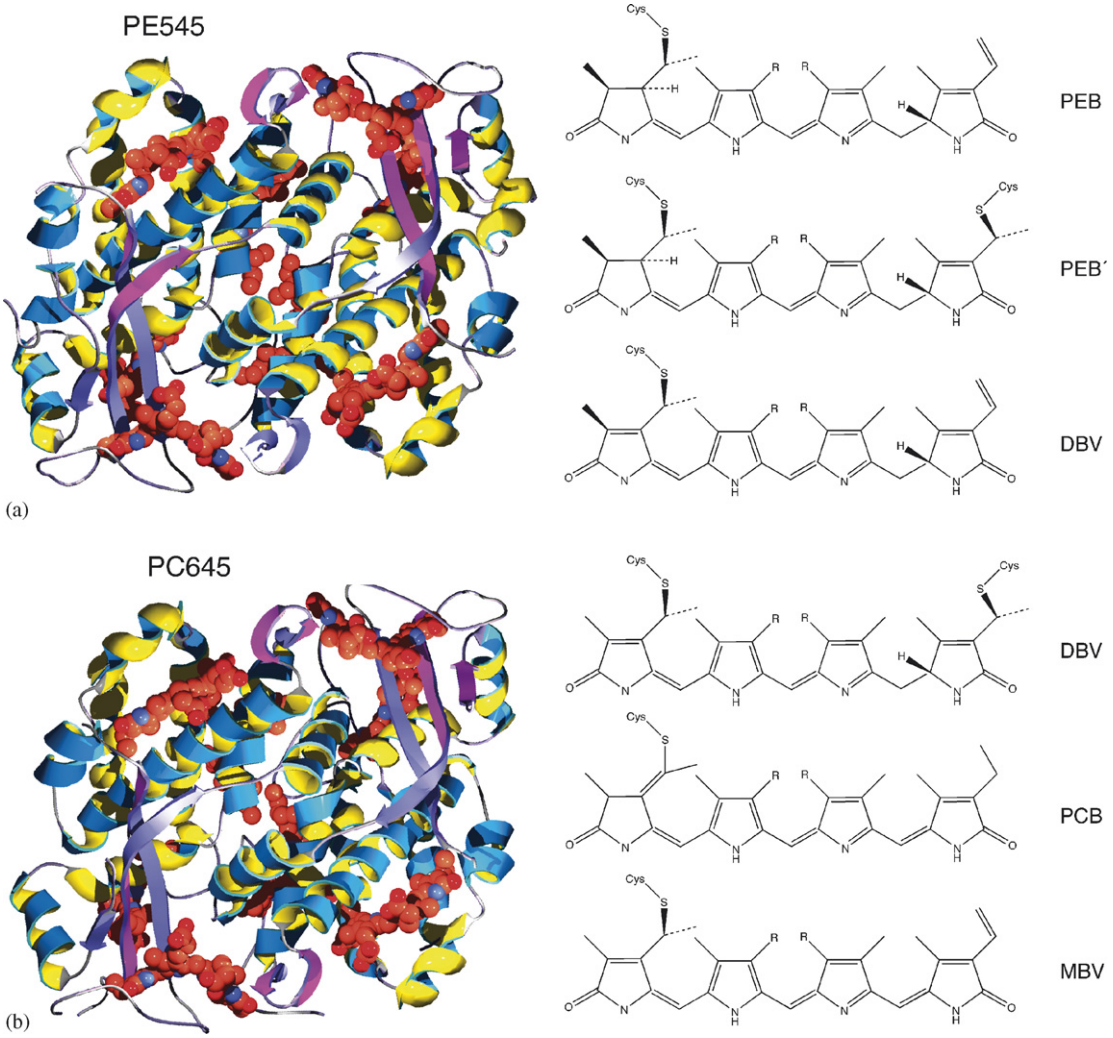

Fig. 3. (a) Structural model of PE545 [59], showing the protein structure and chromophores (red). (b) The chemical structures of the bilins of phycoerythrin 545. R = –CH_2CH_2COOH. Top, the standard PEB chromophore as per β82 and β158; middle, the doubly linked β50/60; and bottom the α19 chromophore. (c) The structure of PC645 at 1.4 Å atomic resolution. (d) The chemical structures of the bilins in PC645. Top, the doubly linked β50/61 DBV chromophore, middle, the singly linked β82 and β158 PCB chromophores, and bottom, the α19 MBV chromophores.

where the numbers indicate the cysteine residues to which the chromophores are linked. The β50/β61 chromophores are linked to two cysteine residues, via their A and D pyrroles. Each α subunit contains a covalently linked 15,16-dihydrobiliverdin (DBV) chromophore, $\alpha_1$19 and $\alpha_2$19, respectively, where each chromophore is covalently linked to Cys-α19 [59]. The extra conjugation in the DBV pigment means its absorption is red-shifted compared to that of the PEBs.

Each of the chromophores is influenced by the surrounding protein structure. Spectral tuning of each chromophore is caused by the local charge environment, interactions with protein ligands, the distortion of the chromophore structure caused by steric effects and restriction of chromophore flexibility [59]. For example, the twisting of adjacent pyrrole rings within a chromophore is chiral and the sign of this twist has been reported [59]. Difference maps show that at least one (and possibly both) of the two central nitrogen atoms of the PEB bilins are usually protonated.

2.2. *Steady-state spectroscopy*

The absorption, circular dichroism (CD) and fluorescence excitation spectra for PE545 recorded at 294 K are shown in Fig. 5 [59]. The absorption spectrum shows a main absorption band at 545 nm and a red shoulder at 567 nm [61], which can be attributed to the DBV pigments. The relatively narrow emission spectrum shows a main emission peak at 579 nm attributed to emission from the lowest energy DBV bilin. The excitation spectrum (monitoring 585 nm emission), corresponds closely to that of the absorption lineshape. At 77 K, the spectra are narrower than the room temperature spectra and allow better distinction of the constituent absorption bands. The position of the main emission band is blue-shifted to 577 nm, and two minor bands at 610 and 634 nm. According to our modeling of the spectra, these latter features are attributed to vibronic structure corresponding to modes with frequencies around 700–800 cm^{-1}.

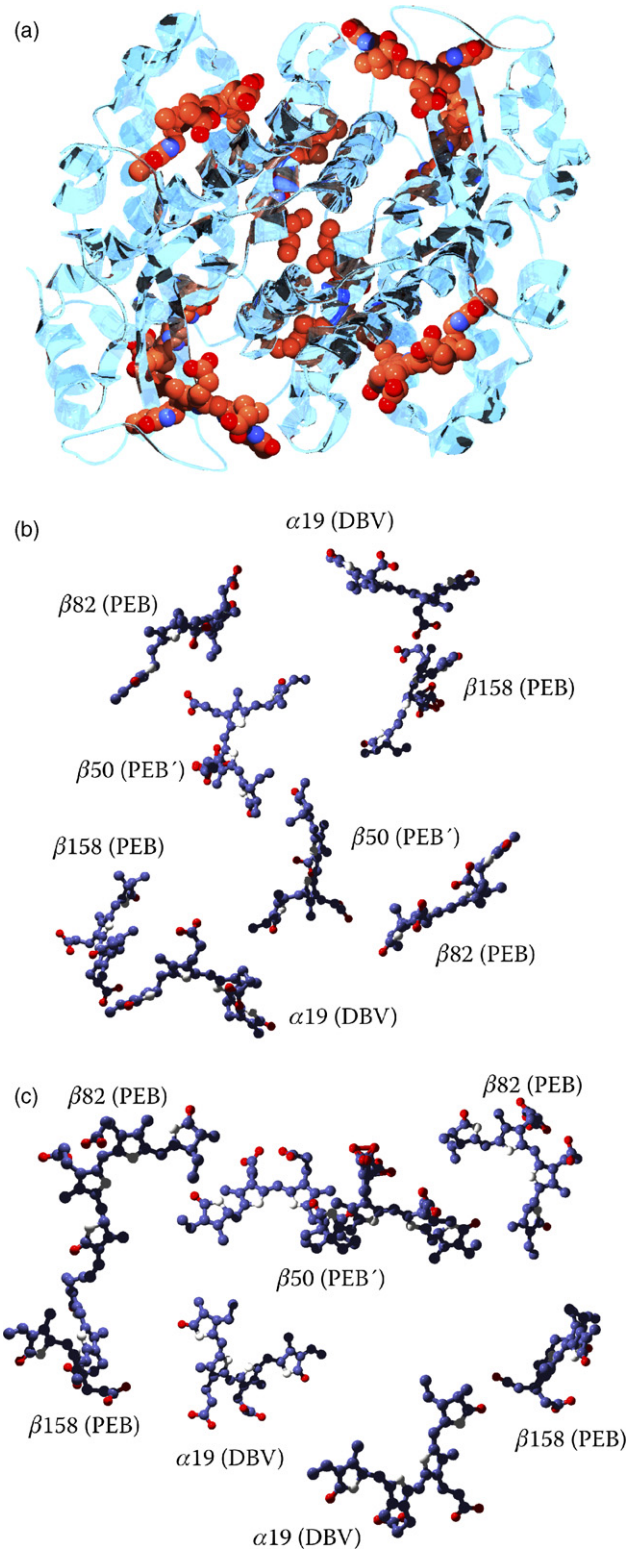

Fig. 4. Arrangement and labeling of the eight bilin chromophores in PE545. (a) and (b) View from above; (c) view from side.

The CD spectrum of PE545 [62–64] is shown in Fig. 5(b). It clearly reveals exciton splitting, evidenced by the characteristic derivative-like feature. The zero-crossing point corresponds closely to the absorption maximum of PE545. The spectrum is not conservative, and that is likely because some of the CD signal is due to the inherent chirality of the bilins. The intrinsic CD expected for the bilins was confirmed by quantum chemical calculations, as outlined in Section 2.4. They are predicted to have rotatory strengths comparable to those for typical chiral molecules [65,66].

The room temperature and 77 K polarization anisotropy measurements were recorded and were found to be similar, meaning that at both temperatures the rotational diffusion is slow compared to the excited state lifetime [62]. The fluorescence polarization excitation spectrum, Fig. 5(c), shows several polarization transitions, including those found at 530 and 560 nm. The spectral difference between the two red DBV bilins is especially clear in the 77 K polarization anisotropy spectrum, where there is a separation of polarization values for the two bilins between 555 and 585 nm. The experimental anisotropy value of 0.175 at 565 nm is consistent with the relative dipole moment angle of 144° between the two DBV bilins, according to $r_0 = (2/5)(3\cos^2\alpha - 1)/2$. Considered together with the highly polarized anisotropy value of 0.38 measured on the red edge of the spectrum, this provides proof that the emission is predominantly from one bilin only. This is surprising, as the distance between the two DBV chromophores is ∼45 Å. We discuss this observation further below.

2.3. Ultrafast spectroscopy

Energy transfer dynamics in PE545 were investigated using two complementary ultrafast spectroscopic techniques, transient grating (TG) and transient absorption (TA), that have been described in detail previously [67]. Briefly, TG is an ultrafast time-resolved four-wave mixing nonlinear optical technique, whereby two spatially overlapped and time-coincident (pump) laser pulses create a frequency-dependent population density in the excited state and a hole in the ground state population, thus forming a spatial population grating in the sample that can be destroyed by population kinetics [68–70]. A third (probe) pulse is scattered off this grating into the Bragg angle. The decay of the grating reflects the loss of excited state population from within the laser spectral window. The ultrafast laser pulses (22 fs) have broad spectra (∼30 nm wide), thus they probe a significant fraction of the absorption spectrum. The population dynamics and energy transfer timescales from both TG and transient absorption techniques were unraveled by global analysis [71–73], and multiexponential fitting of the traces [74,75].

Typical TG data are shown in Fig. 6(a). Note that the intensity scale is logarithmic, and that the traces are normalized near time zero. Most of the dynamics, attributed to energy transfer events that remove population from the probe laser window, occur within the first 50 ps. It is clear from the transient grating results that at higher energy excitation, the fast decay components dominate the kinetics, consistent with a rapid “down hill” energy transfer to red pigments. The timescales observed at all wavelengths are very similar in that there is a near nanosecond timescale, plus faster ∼35, ∼5 and ∼1.8 ps decay components. Oscillations were observed over the first picoseconds, and these decaying, modulated portions of the TG traces were fit to damped cosinusoids using a linear prediction, singular-value-

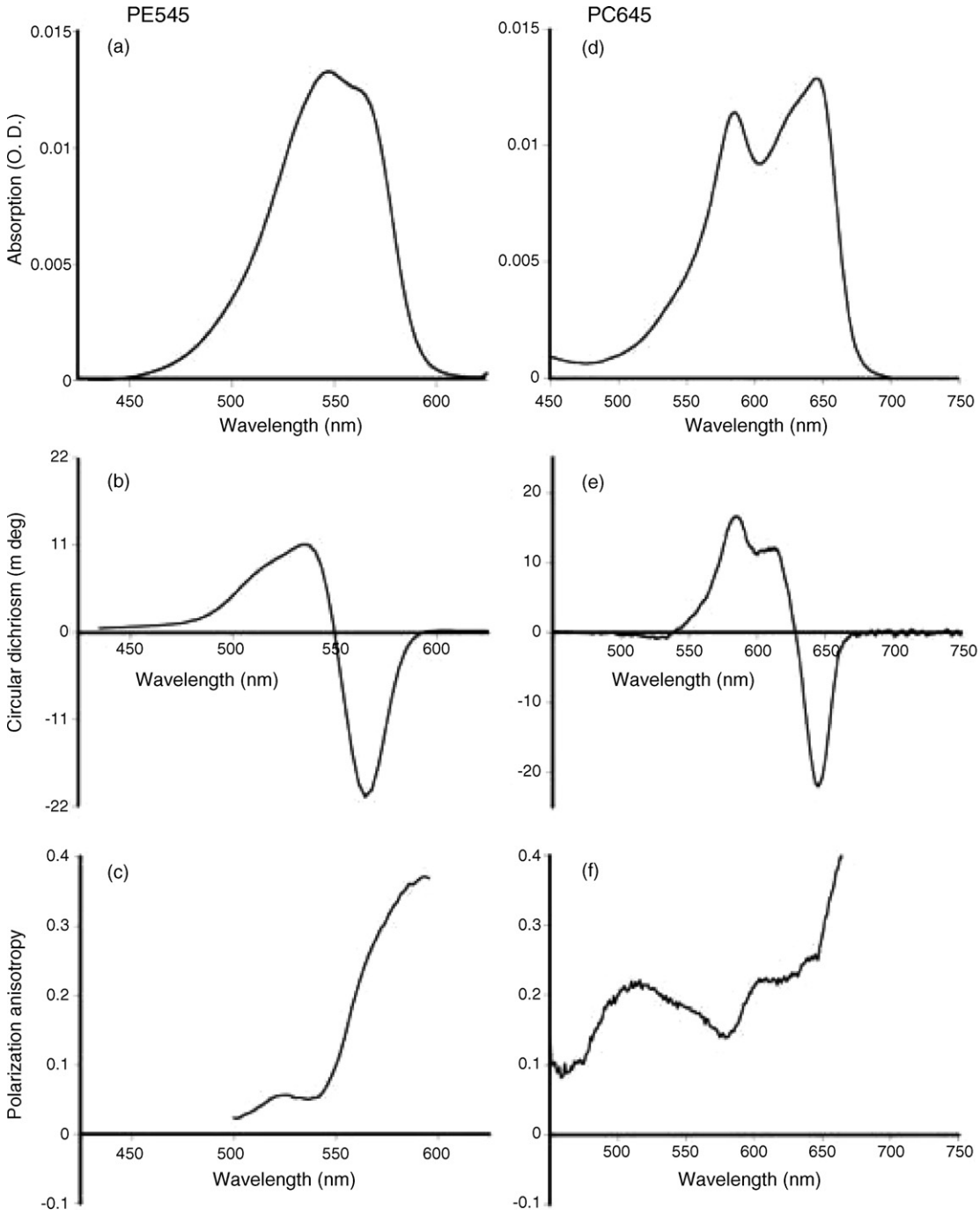

Fig. 5. (a) Absorption spectrum of PE545. (b) Circular dichroism spectrum of PE545 taken from Ref. [8]. (c) Polarization anisotropy of the excitation of PE545 in buffer/glycerol at room temperature. Emission at 615 was monitored for the excitation spectrum and it was corrected for the effects of scatter and birefringence. (d) Absorption spectrum of PC645. (e) Circular dichroism spectrum of PC645. (f) Polarization anisotropy of the excitation of PC645 in buffer/glycerol recorded at room temperature. Emission was monitored at 670 nm.

decomposition procedure [74]. Definitive assignments have not been made, but those frequencies are likely to correspond to low frequency modes of the chomophores. Quantum beats with this range of frequencies seem to typify many antenna complexes [19,76–78].

Transient absorption measurements in combination with a target analysis were pursued in collaboration with the van Grondelle group to attempt to understand more thoroughly the light-harvesting dynamics in PE545. By employing a white-light continuum probe, transient absorption enables examination of the evolution of the energy transfer dynamics in PE545 over the entire spectral range. This is especially important for a definitive assignment of dynamical processes in PE545 since spectral congestion is significant. Excitation wavelengths were chosen to be 485 and 530 nm, and a probe window between 400 and 700 nm was measured up to a maximum delay of 200 ps.

The transient absorption spectra consist of a positive peak centered around 450 nm due to excited state absorption (ESA)

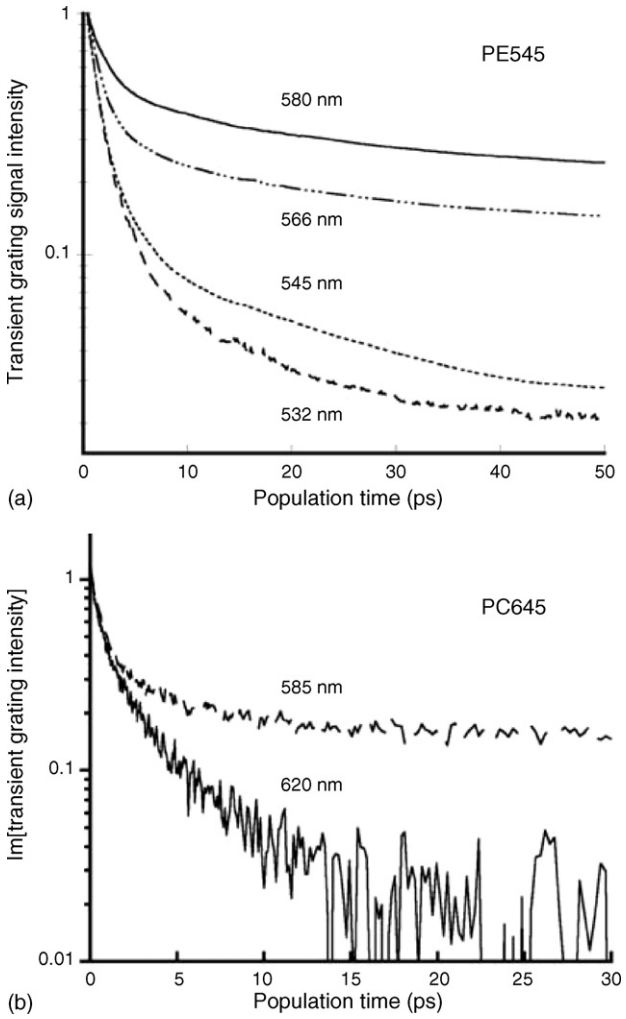

Fig. 6. (a) Wavelength-dependent transient grating data for PE545 at room temperature. Excitation wavelengths from top to bottom are 580, 566, 545 and 532 nm, respectively. (b) Wavelength-dependent transient grating population decay data for PC645 at room temperature. Excitation wavelengths are 585 and 620 nm (as indicated). The data have been normalized at 150 fs (i.e. after pulse overlap).

and negative signals between 480 and 640 nm reflecting contributions of the ground state bleach (GSB) and stimulated emission (SE). Beyond 640 nm, there is an additional ESA contribution to the transient absorption spectra. Each data set was globally analyzed using an evolutionary kinetic scheme. Five lifetimes were needed to obtain a satisfactory fit over all data sets. The first lifetime was arbitrarily set to 25 fs because it was too rapid to be precisely estimated. The lifetime of the long-lived state was greater than 1 ns (the fluorescence lifetime of the emitting α19 bilin is 2.5 ns at room temperature), but could not be estimated accurately owing to the limited experimental time window of 200 ps. The 77 K data sets provided excellent spectral resolution owing to the narrowed spectral bands, as described in detail elsewhere [79].

Immediately after excitation, the transient differential transmission spectra transform very rapidly (∼25 fs). Most of the excitation becomes localized on the lowest exciton state of the dimer and the other PEB bilins. This spectral feature transforms into another transient spectrum associated with global kinetic evolution on a time scale of 250 fs at room temperature (or about a picosecond at 77 K). It was found that, although most of the excitation has at that point reached the red DBV bilins, there is still some residual excitation of the 550 nm state, especially at room temperature. That equilibration of the excitation energy is notably rapid. The excited state population then transforms into the penultimate spectral signature in under 2 ps at room temperature (3 ps at 77 K), which concurs with the depletion of excitation of the 550 nm state. At this time all the excitation is localized on the red DBV bilins. A final energy transfer time is associated with a red shift of the bleach to 575 nm. In that step all the energy accumulates on the red-most DBV bilin over ∼24 ps (485 nm excitation) and 16.4 ps (530 nm) at room temperature. At 77 K those time scales are found to be 30 ps (485 nm) and 18 ps (530 nm).

2.4. Quantum chemical calculations

Gaussian 03 [80] was employed to calculate the excited state properties [81] of each of the eight bilins in PE545. Atomic coordinates were taken from the 0.97 Å resolution crystal structure model [59]. In the apoprotein a thioether linkage links each of the tetrapyrroles to the protein. We included the sulfur, but replaced the covalent bond to the protein with a hydrogen atom. The excited state wave functions were obtained using configuration interaction with single excitations from a spin restricted Hartree–Fock (6-31G basis set) reference determinant (the CIS method) [82]. The results of these calculations are summarized in Table 1. The two DBV bilins were found to be the lowest energy bilins, as expected, with transition dipole moments calcu-

Table 1
The results of the excited state calculations on the bilins of PE545 and PC645 using the CI-singles method and a 6-31G basis set

PE545			PC645		
Bilin	Excitation energy (eV)	Transition dipole moment (D)	Bilin	Excitation energy (eV)	Transition dipole moment (D)
DBV α19-A	3.15	11.6	MBV α19-A	2.87	9.28
DBV α19-B	3.04	8.78	MBV α19-B	2.92	6.06
PEB β50/61-C	3.47	9.42	DBV β50/61-C	3.16	10.9
PEB β50/61-D	3.53	16.0	DBV β50/61-D	3.17	14.6
PEB β82-C	3.25	3.46	PCB β82-C	2.57	5.45
PEB β82-D	3.28	5.31	PCB β158-D	2.57	9.96
PEB β158-C	3.30	9.68			
PEB β158-D	3.38	8.11			

lated to be between 3.5 and 16 D. The transition dipole moment vectors are oriented across the three conjugated pyrrole units.

The Coulombic electronic couplings that promote resonance energy transfer between the bilins were evaluated using the transition density cube (TDC) method [33,83,84]. Transition density cubes (TDCs) were calculated for each bilin. The TDC for a molecule contains all the information needed to calculate integrals involving that transition density (e.g. between ground and first excited state). For example, the Coulombic integral via which excitation energy is exchanged between molecules is such a two-electron integral [32,33,37,83]. An isosurface plot of a TDC is shown in Fig. 7 together with an illustration of the principle of the TDC method for calculating interchromophore interactions. If the dipole operator acts on a TDC, then the transition dipole vector is obtained. If the interaction between two such transition dipoles is calculated, then the electronic coupling calculation reduces to the point dipole approximation. That is the well-known dipole approximation, which is useful when the separation between the two chromophores is significantly greater than their sizes. The TDC method avoids this approximation by calculating the interaction between the transition densities directly.

The results of our electronic coupling calculations are collected in Table 2. These couplings have been scaled to the experimentally measured transition dipole magnitude of 11.25 D. That transition moment equates to a molar extinction coefficient of $6.84 \times 10^5\ \mathrm{cm^{-1}\,M^{-1}}$, and compares with other reports in the literature [85]. The scaling procedure corrects for the typical overestimation of the transition moment magnitude by CIS calculations, and is described in Ref. [33]. The value of 11.25 D was assumed to be equal for all bilins. However, the calculated transition dipole strengths reported in Table 1 show marked variation, which depends strongly on the bilin conformation in the protein. Further work in conjunction with experiment is necessary to assign average transition dipole moment magnitudes to each bilin in the protein. At that point the electronic couplings can be refined. Electronic couplings between all pairs of bilins in PE545 were calculated in this manner. We found that they range from $<5\ \mathrm{cm^{-1}}$ (for α19-B to β158-C) to $304\ \mathrm{cm^{-1}}$ for the interaction between the PEB′ chromophores that constitute the central dimer.

To evaluate the effect of deviations from the dipole approximation we consider the electronic coupling correction factor $\eta = (V/V_{\mathrm{dip-dip}})^{1/3}$ [40], where V is the electronic coupling between the donor and acceptor calculated using the TDC method and $V_{\mathrm{dip-dip}}$ is the coupling calculated according to the dipole approximation. We find that for interchromophore distances greater than 40 Å, the dipole approximation is adequate for describing the electronic coupling. Even between 25 and 40 Å most of the TDC electronic couplings are similar to $V_{\mathrm{dip-dip}}$, and η is found to be between 0.9 and 1.1. With $\eta = 0.9$ the energy transfer rate is found to be only ∼25% of that predicted using the Förster equation. When $\eta = 1.1$ the rate is increased by ∼75% over the Förster theory prediction, so the corrections due to deviations from the dipole approximation can be significant. Two notable cases are β50/61-C to β158-D ($\eta = 0.68$) and α19-B to β158-D ($\eta = 1.18$). In these instances the dipole approximation does not capture details of the shape of the interaction, which is likely to be because the bilins lie close together and at an awkward orientation. In one case the bilins appear to be arranged in a herringbone type perpendicular orientation and for the other, the bilins have a staggered parallel orientation.

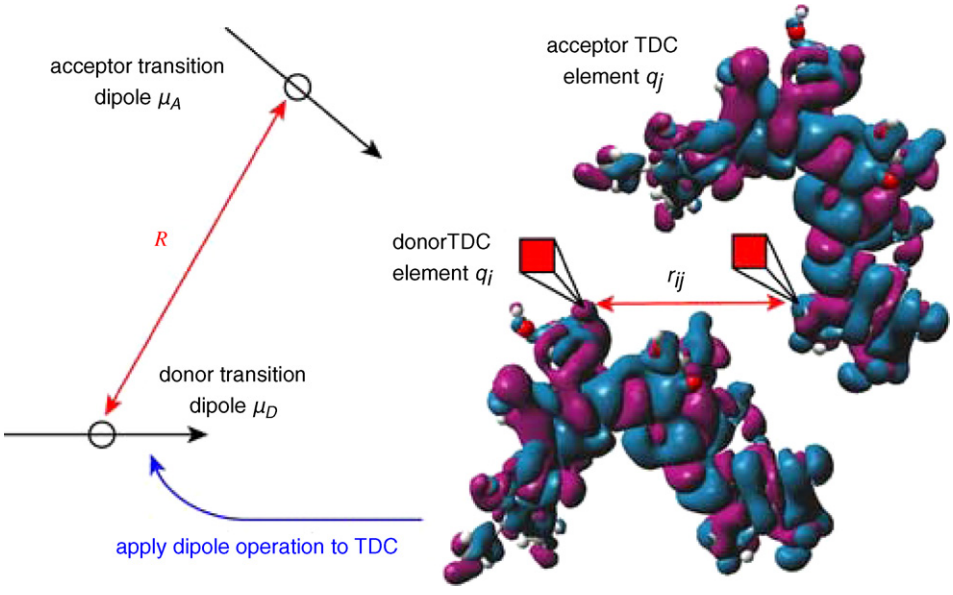

Fig. 7. The electron density for the ground to excited state transition of the SLA2 bilin in PE545 is shown plotted in a schematic description of the transition density cube (TDC) method for calculating interchromophore interactions. The TDC is made up of many small charge elements, shown as the red squares. Each charge element on the donor interacts with each charge element on the acceptor via the Coulomb interaction. The sum of those interactions provides an accurate account of the interchromophore coupling by retaining details of the shape of each transition density and therefore how each molecule "sees" the other on an atomic length scale. In contrast, while an interaction between transition dipoles usually provides a reasonable estimate of the electronic coupling, it can fail completely when it is not able to capture essential details of the transition density shapes.

Table 2
The electronic couplings calculated between the bilins of PE545 using the TDC method, where $V_{dip-dip}$ is the coupling calculated using the dipole approximation and V is the TDC coupling (scaled using a transition dipole moment magnitude of 11.25 D, see text for explanation)

Donor transition	Acceptor transition	Separation (Å)	Orientation factor, κ	$V_{dip-dip}$ (cm^{-1})	V (cm^{-1})
α19-A	α19-B	44.64	−0.851	−6.10	−5.43
α19-A	β50/61-C	30.57	0.241	5.38	6.93
α19-A	β82-C	33.84	1.016	26.70	16.98
α19-A	β158-C	20.47	0.533	−39.65	−51.92
α19-A	β50/61-D	22.87	−1.081	−57.57	−51.71
α19-A	β82-D	23.21	1.402	71.45	78.79
α19-A	β158-D	45.91	−0.41	−2.70	−2.76
α19-B	β50/61-C	23.61	−1.081	−52.27	−48.09
α19-B	β82-C	23.29	1.393	70.29	67.43
α19-B	β158-C	46.40	−0.715	−4.56	−4.77
α19-B	β50/61-D	30.26	0.228	5.24	6.16
α19-B	β82-D	34.36	1.274	20.00	16.46
α19-B	β158-D	19.95	−0.646	−51.83	−83.04
β50/61-C	β82-C	22.01	−0.819	−48.94	−58.26
β50/61-C	β158-C	24.21	−0.233	−9.99	−11.63
β50/61-C	β50/61-D	15.10	1.34	247.80	304.14
β50/61-C	β82-D	32.77	0.651	11.78	10.14
β50/61-C	β158-D	21.83	−0.172	−10.29	−3.11
β82-C	β158-C	35.79	−0.698	−9.69	−11.90
β82-C	β50/61-D	31.12	1.203	25.42	30.97
β82-C	β82-D	35.32	−0.657	−9.49	−7.97
β82-C	β158-D	36.59	0.793	10.32	8.24
β158-C	β50/61-D	22.26	−0.566	−32.70	−33.65
β158-C	β82-D	37.92	1.226	14.33	15.54
β158-C	β158-D	42.19	0.886	7.14	7.40
β50/61-D	β82-D	22.65	−0.911	−49.94	−44.68
β50/61-D	β158-D	24.19	−0.412	−18.55	−21.61
β82-D	β158-D	36.75	−0.916	−11.76	−10.63

In order to predict energy transfer times between the bilins in PE545, realistic spectral line shapes for the absorption and emission of each bilin must be deconvoluted from the absorption spectrum because these are required to estimate spectral overlaps. Once these line shapes are known, realistic generalized Förster theory calculations can be carried out as described in detail for energy transfer in LH2 [86] and other molecular assemblies [21,32,87]. In that way excitonic effects among acceptor molecules are captured by the calculations. Such electronic interactions among the acceptors may have significant qualitative, as well as quantitative, consequences for the mechanism and rate of electronic energy transfer. In our calculations, electronic couplings are taken from TDC calculations and spectral overlaps are determined by first calculating spectral line shapes for each chromophore type [88–92]. An important motivation for such calculations of energy transfer dynamics is that, in conjunction with the timescales extracted from ultrafast experiments, a detailed model can be elucidated that relates a dynamical model to the structural model provided by the crystallographic data.

The absorption and circular dichroism spectra of PE545 were simultaneously simulated to obtain the spectral line shape of the protein as a sum of contributions from essentially individual chromophores and collective (exciton) states resulting from electronic coupling among the chromophores. In particular, simulation of the essential features of the CD spectrum provides support for the accuracy of the quantum chemical calculations and the associated spectral model, since the CD spectrum is highly sensitive to the magnitude of the electronic couplings and the orientation of the transition dipole moments. With that information, energy transfer rates were calculated, as will be reported in detail elsewhere. It is clear that there are multiple paths for energy transfer in PE545, and modeling of individual energy transfer rates needs to be combined with an overall kinetic analysis in order to compare with experiment. The experimental studies showed that excitation equilibrates among the PEB chromophores within the protein in a few hundred femtoseconds. In the next time regime, energy is transferred from the peripheral PEBs to the dimer, which takes 0.5–5 ps. That is an interesting case where a correct prediction of the energy transfer dynamics can only be achieved by using generalized Förster theory.

Here we focus our discussion on the final energy transfer step. Using Förster theory, Eq. (1b) with a carefully determined spectral overlap integral J and the TDC electronic coupling V we estimate the final DBV to DBV energy transfer step to occur in 76 ps. However, the experimental results suggest this time to be ∼25–30 ps. We show below that the electronic coupling involves both a direct interaction, as we obtained from the Förster-type calculation, and an additional, superexchange, contribution. The overall electronic coupling then is the effective coupling V_{eff}. By considering the ratio of the measured rate to the TDC-Förster

rate, together with the Fermi golden rule, we anticipate that $V_{\mathrm{eff}} \approx 1.7\, V_{\mathrm{direct}}$, where $V_{\mathrm{direct}} = V$ is the direct electronic coupling between α19-B and α19-A, calculated using the TDC method.

An explanation for the meaning of V_{eff} and hence the discrepancy in measured and calculated energy transfer rates can be suggested from inspection of Table 2 and Fig. 8. Intermediate between the peripheral DBV bilins are other chromophores that couple quite strongly to each DBV bilin. For example, α19-B couples to β50/61-C ($-48\,\mathrm{cm}^{-1}$), β50/61-C couples to β50/61-D ($304\,\mathrm{cm}^{-1}$), and that, in turn, couples to α19-A ($-52\,\mathrm{cm}^{-1}$). Such bridging of electronic couplings provides superexchange-mediated interactions coupling α19-B to α19-A [21,32,39]. The sequence of possible pathways for such coupling is complicated, and each pathway may either increase or decrease the overall α19-B to α19-A "effective" electronic coupling, according to the nature of interferences. It turns out that the outcome of a calculation of the effective α19-B to α19-A coupling for PE545 depends critically on the site energies of the PEB′ dimer bilins. Our calculations suggest that perhaps their energies are unequal, but further work is required to refine our model.

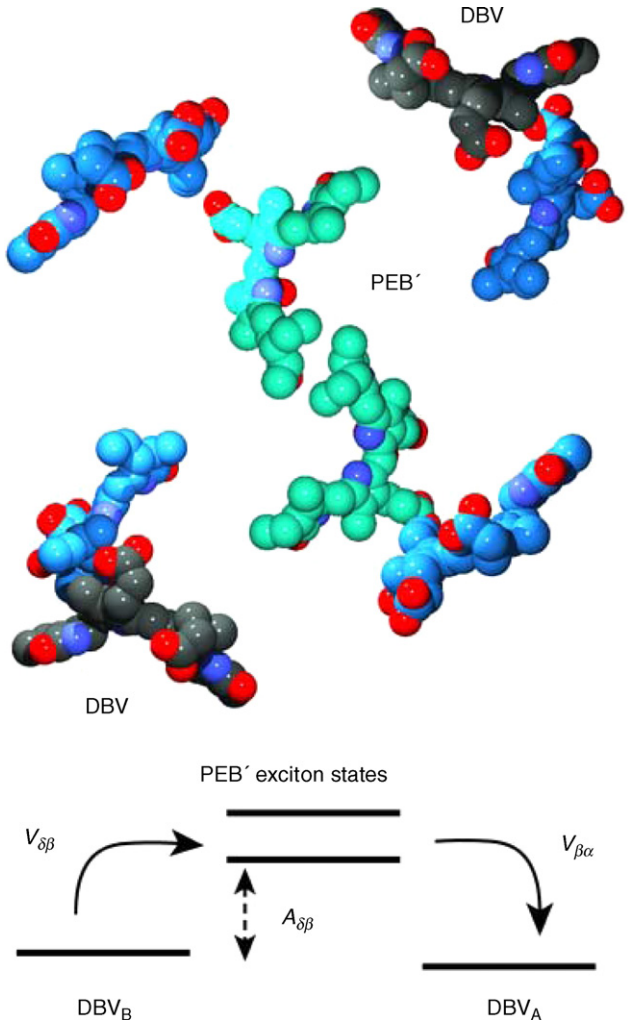

Fig. 8. Top shows the spatial arrangement of the DBV chromophores (charcoal) and the dimer "bridge" (green). Bottom shows a schematic of the donor and acceptor DBV states and the intermediate "effective" bridge states $|\beta\rangle = (|b_1\rangle \pm |b_2\rangle)/\sqrt{2}$ (when each PEB′ site energy is identical) that mediate the superexchange interaction. $A_{\delta\beta}$ is the donor-bridge energy gap. For perturbation theory to describe the effective donor–acceptor electronic coupling $V_{\delta\alpha}$, it is necessary that $V_{\delta\beta}, V_{\beta\alpha} \gg A_{\delta\beta}$.

Superexchange-mediated electronic coupling can easily be estimated using perturbation theory [39], but it is more accurate to calculate the effective coupling directly—particularly given the complexity of the system. To do that we take the entire Hamiltonian and use a Löwdin partitioning method to find the effective donor $|\alpha\rangle$ and effective acceptor $|\beta\rangle$, as has been described by one of us previously [21,32,37]. To illustrate that we consider just a simple model system comprised of the two DBV bilins and the PEB′ dimer. The excited state of the donor DBV (α19-B) is labeled $|d\rangle$, that of the acceptor DBV (α19-A) is $|a\rangle$, and each PEB′ bilin of the dimer is $|b_1\rangle$ and $|b_2\rangle$. Diagonalizing the partitioned Hamiltonian with the excitation energy of each PEB′ set to be $916\,\mathrm{cm}^{-1}$ above the donor DBV, and the acceptor DBV red-shifted by $185\,\mathrm{cm}^{-1}$ from the donor, yields the effective donor and acceptor states:

$$|\delta\rangle = 0.9978|d\rangle + 0.0611|b_1\rangle - 0.0269|b_2\rangle,$$

$$|\alpha\rangle = 0.9984|a\rangle - 0.0207|b_1\rangle + 0.0525|b_2\rangle$$

Expanding and evaluating the matrix element $V_{\delta\alpha}$ with the aid of the site couplings listed in Table 2 obtains the effective electronic coupling,

$$V_{\delta\alpha} \equiv V_{\mathrm{eff}} = \langle\alpha|H|\delta\rangle = -3.7\,\mathrm{cm}^{-1} \quad (6)$$

Notice that the superexchange pathway interferes destructively with the direct coupling ($V_{\mathrm{da}} = -5.4\,\mathrm{cm}^{-1}$) to reduce the overall coupling. By lowering the energy of either PEB′ state, or both of them, V_{eff} can be increased relative to V_{da}. At the present time we are still refining the model, but the demonstration that superexchange-mediated electronic coupling can occur, so that interaction among the DBV bilins is bridged by the intervening chromphores, is interesting.

2.5. A model for energy transfer

From the analysis of the transient grating and transient absorption measurements, the dynamics within the strongly coupled central PEB dimer were unresolvable. That is not surprising given that for systems such as the reaction center special pair, LH2, or the allophycocyanin trimer, the exciton relaxation dynamics are of the order of tens of fs. For example, interexciton-state relaxation in the dimer in allophycocyanin occurs on a ∼30 fs timescale [92]. Ultimately, from the dimer trap, the excitation is transferred from the center of the protein to the periphery. Besides the sub-pulse width dynamics of the dimer, some of the predicted energy transfer rates from the β158 and β82 PEB bilins to the lowest exciton state of the dimer and DBV bilins are also ultrafast and would not be directly detectable in our experiments on PE545.

Fig. 9 summarizes the dynamic processes in PE545 that were observed by the ultrafast measurements and relates those dynamics to structure and spectra. That is possible as a result of the detailed quantum mechanical calculations of energy transfer

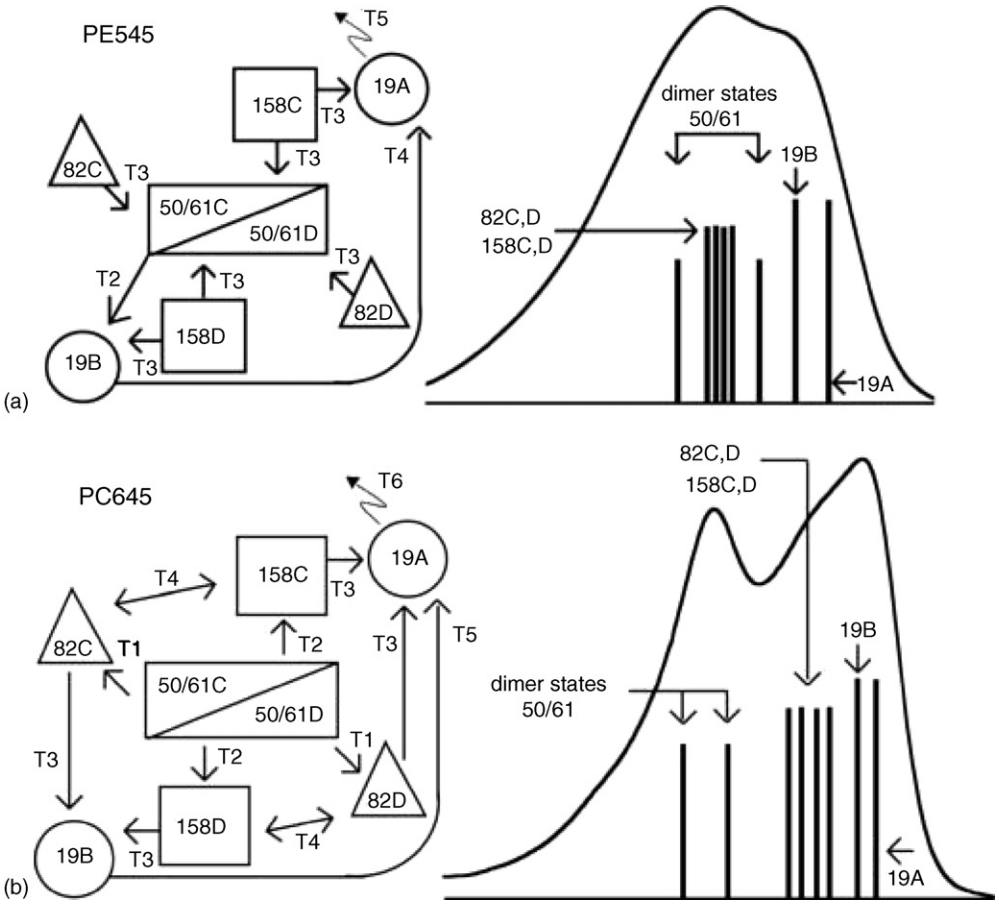

Fig. 9. (a) A model of energy transfer in PE545 (left panel), and spectral positions of the bilins in PE545 (right panel). Excitation is funneled from the peripheral PEB bilins to the central dimer from where it is transferred to the DBV bilins. Rates *T*2, *T*3, and *T*4 refer to the time scales elucidated from analysis of the transient absorption data, and *T*5 is the fluorescence lifetime of the emitting bilin. (b) A qualitative model for energy transfer in PC645 (left panel), and the spectral positions of the bilins in PC645 according to the present model (right). Excitation is transferred from the DBV dimer to the PCBs, from where the excitation is directed to the lowest energy MBV bilins. Rates *T*1 to *T*5 represent possible energy transfer timescales, and *T*6 is the fluorescence lifetime of the emitting bilin *in vitro*.

dynamics described above. The bilins have been divided into three groups; the central dimer PEB bilins (β50/β61), the PEB bilins (β158, β82) and the DBV bilins (α19). The structure is shown schematically. The time constants T_n are those retrieved from the detailed global analysis of the transient absorption data.

The first process that occurs at sub-pulse width time resolution is the internal conversion from the high to the low exciton state of the central dimer, which is part of *T*1 set at 25 fs. Population in the lowest exciton state of that dimer transfers to the blue-most DBV bilin in around 250 fs (*T*2). Owing to very similar timescales and spectral features, it is difficult to separate individual energy transfer routes between the eight bilins in PE545. These energy transfer processes are collectively seen as *T*3 (0.5–5 ps). It is predicted that *T*3 encompasses the following energy transfers: the β158 and β82 bilins to the lowest exciton state of the central dimer (β50/β61C), as well as direct energy transfer of β158D to α19B and β158C to α19A, which is arbitrarily chosen to be the DBV bilin responsible for emission. Owing to the symmetry of PE545, this assumption is a fair one. The final energy transfer step, *T*4, results in all the excitation ending up on the final emitting DBV bilin. It is also concluded that there is no energy transfer between the β158 and β82 bilins. The existence of the central dimer in PE545 is important in this organism as it relies on just two bilin types to cover the same part of the spectrum, which in cyanobacteria and red algae is covered by multiple proteins and bilins in the phycobilisome structures. The dimer in PE545 expands spectral coverage, ensures more efficient trapping of energy, and mediates the ensuing transfer of this excitation to the red DBV bilins.

3. Phycocyanin 645

3.1. Structure

The crystal structure of Phycocyanin 645, Fig. 3, was determined at 1.4 Å atomic resolution, and was found to be very similar to that of PE545, the root mean square distance comparison being 0.9 Å for C_α atoms. The chromophores were also found to be located in similar positions to those in PE545. It is interesting to note that the central pair of bilins are even closer together than in PE545, with the rings stacked in a staggered fashion. The major difference between PE545 and PC645 is the chemical composition of the tetrapyrrole phycobilin chromophores [93]. PC645 contains three different types of bilins: two 15,16-

dihydrobiliverdins (DBVs), two mesobiliverdins (MBVs) and four phycocyanobilins (PCBs). According to the present structural model, the MBVs are located on both α-subunits at the α19 position, the DBVs on both β-subunits at the central doubly bound β50-61 position and the PCBs on both β-subunits are at β82 and β158.

3.2. Steady-state spectroscopy

The longer conjugation lengths of the PCB bilins result in lower energy transitions and the consequent red-shift differentiates PC645 spectroscopy from that of PE545. This also explains the blue appearance of PC645 versus the pink colour of PE545. The absorption spectrum, Fig. 5(d), shows bands at 585 and 645 nm, and a shoulder at 620 nm. The blue peak at 585 nm is attributed to the two dihydrobiliverdin (DBV) bilins. These are the only chromophores common to both PC645 and PE545. The absorption bands under the 620 nm shoulder are attributed to the four phycocyanobilins (PCB) [94–96]. The red peak at 645 nm is assigned to the emitting bilins, two mesobiliverdins (MBV), which are found on the α-subunits. The fluorescence emission spectrum has a peak at 662 nm at room temperature and a shoulder at 735 nm, assigned to a vibrational sub-band. We suggest that the energy transfer from PC645 to membrane bound chlorophylls should to be more efficient for PC645 compared to PE545 because of significantly better spectral overlap between PC645 emission and Chl *a* absorption.

The CD spectrum of PC645, Fig. 5(e), is rather complex. Two pairs of positive and negative bands, indicative of exciton splitting, can be discerned; see the large negative band on the red edge, and a much smaller, but definitely negative band on the blue edge. The zero-crossing of the red edge feature is at 620 nm, which corresponds to the absorption maxima of the PCBs. It seems that the blue edge negative band is due to the DBV β50/β61 central dimer, and the red edge negative band signifies excitonic interactions among the PCB bilins. Perhaps the latter feature includes the MBV bilins on the α-subunits, because the red-most bilins in PE545 were also seen to contribute to the negative CD in its spectrum. The large positive bands in the CD spectrum of PC645 sandwiched in between the split positive and negative bands, together with the fact that the spectrum is not conservative, indicate that some of the CD signal is due to the inherent chirality of the bilins [18,97].

The polarization anisotropy excitation data, Fig. 5(f), show several polarization transitions, at 470, 510, 585, 600 and 645 nm. The anisotropy is only ∼0.14 at 585 nm, corresponding with the absorption peak attributed to the DBV bilins, which are spectrally distinct from the other chromophores. The polarization anisotropy then increases at lower wavelength to a value of $r \sim 0.2$ for the four PCB bilins. As in the case of PE545, the spectral difference between the two red-most bilins is clear at 645 nm, where $r = 0.21$ at 77 K and 0.25 at room temperature. That compares with the value of 0.25 reported by Csatorday et al. for room temperature [96]. Finally, just as in PE545, it can be concluded for PC645 that there is a single emitter. That is evidenced by the peak polarization anisotropy of ∼0.4 at the red edge of the absorption spectrum.

3.3. Ultrafast spectroscopy

Transient grating experiments were also performed for PC645, but for these measurements we employed optical heterodyne detection (OHD-TG) [98–101]. The key difference from the setup described in Section 2.3 is that phase-locked pulse pairs were used. The signal was overlapped with one of these four beams, the local oscillator, in order to linearize the detected signal intensity. By adjusting a phase delay, the real (refractive) and imaginary (absorptive) contributions to the signal could be measured independently. The latter signal contribution is sensitive to population changes. We recorded the decay of the imaginary part to the OHD-TG signal intensity as a function of pump–probe delay time up to a population time of 30 ps, Fig. 6(b). The measurements on PC645 were performed using 20 fs laser pulses (32 nm spectral width) at two excitation wavelengths, 585 and 620 nm.

The OHD-TG traces were simultaneously fit to two exponentials plus a static offset, which fit the data well. At both excitation wavelengths, there is biphasic behaviour in energy transfer, in that there is a fast (566 fs) decay and a slower (3.6 ps) component, which reflects the multiple pathways for the excitation to migrate within the protein. That is hardly surprising considering the number of donor and accepter bilins at these excitation wavelengths. These times are similar to those obtained for PE545.

Individual decay fits were also performed, as the two excitation pulses were sufficiently separated spectrally that it cannot be assumed that they initiate the same dynamical processes. Interestingly, subsequent to 620 nm excitation, the population decay appears faster than after 585 nm excitation. In both cases, however, these dynamics appear to be completed by ∼15 ps. That observation is different from the case of PE545, where the red-most excitations yielded the slowest exponential decays. The final energy transfer step between the blue and red MBV bilins could not be deduced from this experiment, but is expected to be comparable to the DBV to DBV energy transfer step in PE545. The rapidly damped oscillation seen in the 620 nm data at 0–250 fs was fitted to the damped cosinusoid [74] and found to correspond to a vibrational frequency of 208 cm^{-1}.

3.4. Quantum chemical calculations

Gas phase calculations of the excited state properties of six of the bilins: the DBVs, both MBVs, and two of the PCBs, β158C and β82C, were performed using the CI-singles method. The results are summarized in Table 1. The vertical excitation energies for the two DBV bilins were found to be higher energy transitions than those of any other bilins, as expected. Unexpectedly, the PCB bilins were found to have lower vertical excitation energies than the MBV bilins. This perhaps highlights the importance of the role of the protein, the aqueous environment, and indeed the protonation state of the chromophores in tuning excitation energies [24,102,103]. The transition dipole moments were calculated to be between 5.45 and 15 D, similar to the range 3.5–16 D found for PE545.

The electronic couplings between the same six bilins were calculated using the transition density cube method. In scaling

the coupling values to experimental ones, it was decided to use the same 11.25 D value determined for PE545. The couplings are quite similar to the values obtained for the equivalent bilins in PE545 with the exception of the central dimer pair, which was found to have a much larger electronic coupling owing to the closer separation of the chromophores in the PC645 central dimer compared to that in PE545. For that dimer, an inter-pigment distance shortening from 15.1 Å in PE545 to 14.3 Å in PC645 was found to provide a larger electronic coupling within the PC645 dimer of 455 cm^{-1}, compared to 304 cm^{-1} in PE545. The coupling between the two lowest energy bilins was calculated to be smaller in PC645 compared to PE545, but the implication of that for the rate of the final energy transfer step need further investigation.

3.5. A model of energy transfer

As opposed to PE545, the central dimer bilins are spectrally more isolated on the blue edge of the absorption spectrum, making the possible energy transfer pathways somewhat different. A model for energy transfer is suggested in Fig. 9. In it, there are four bilin pairs; the central dimer bilins (β50/β61, rectangle), two sets of PCB bilins (β158, squares; β82, triangles) and the MBV bilins (α19, circles). *T*1 to *T*5 represent possible compartments of timescales and on the right are the expected bilin spectral positions.

The first process that occurs at sub-pulse width time resolution is the internal conversion from the high to the low exciton state of the central dimer. Henceforth, the excitation is transferred to the PCB bilins. Direct dimer to MBV bilin energy transfer is considered unlikely owing to the small spectral overlap. The PCBs are thus responsible for transferring the excitation to the lowest energy MBV bilins. The final energy transfer step, analogous to PE545, sensitizes only one of the MBV bilins. That bilin is the final trap and is responsible for emission.

In Fig. 9, *T*1 and *T*3 represent the fast energy transfer time as obtained in the TG experiment and involves both the transfer of excitation from the lowest exciton state of the central dimer to the β82 bilins as well as all PCBs transferring their excitation to the MBV bilins; β82C and β158D to a19B and β82D and β158C to a19A, which was arbitrarily chosen to be the lowest energy MBV bilin responsible for emission. *T*2 and *T*4 represent the slower subsequent and competing energy transfer processes. *T*5 is the final energy transfer step between the two MBV bilins, but since this part of the spectrum was not covered by the laser pulse spectra in the experiments we have performed so far, it was not determined. *T*6 is the fluorescence lifetime of the emitting bilin, which has been found to be 1.44 ns [104].

4. Intact cryptophyte algae

4.1. Rhodomonas CS24

On the basis of the spectroscopic results on isolated PE545, it is expected that equilibration of the absorbed excitation to the single, red-most DBV bilin in PE545 would precede transfer of excitation into the chlorophyll-containing proteins bound in the thylakoid membrane. However, that model poses the problem that it is difficult to rationalize the observed light-harvesting efficiency for proteins whose emitting bilin is oriented away from the membrane.

In order to determine better the role of PE545 as a light harvesting antenna complex, time-resolved fluorescence from intact *Rhodomonas CS24* algae was measured using a streak camera in combination with a spectrograph which allows the simultaneous detection of decay traces at a great number of wavelengths, providing high resolution in both time and spectral dimensions [48,105–107]. The absorption spectra of *Rhodomonas CS24* algae recorded at room temperature and 77 K are shown in Fig. 10. The second derivative of the 77 K spectrum reveals an abundance of Chl emission bands, and based on previous assignments of the spectral positions of the pigments in cryptophytes [13,50,108,109], it was possible to assign the peak positions. The most dominant Chl *a* peak is at 681 nm, with another band at 672 nm, and the Soret band at 436 nm. Chl *c2* has its Q_y absorption maximum at 642 nm with a Soret band at 471 nm. The carotenoids, mainly alloxanthin, absorb around 500 nm. PE545 absorbs in the region between the carotenoids and the Q_y absorption bands of the Chls.

Fig. 11 shows fluorescence emission spectra of the algae at room temperature for two selected excitation wavelengths.

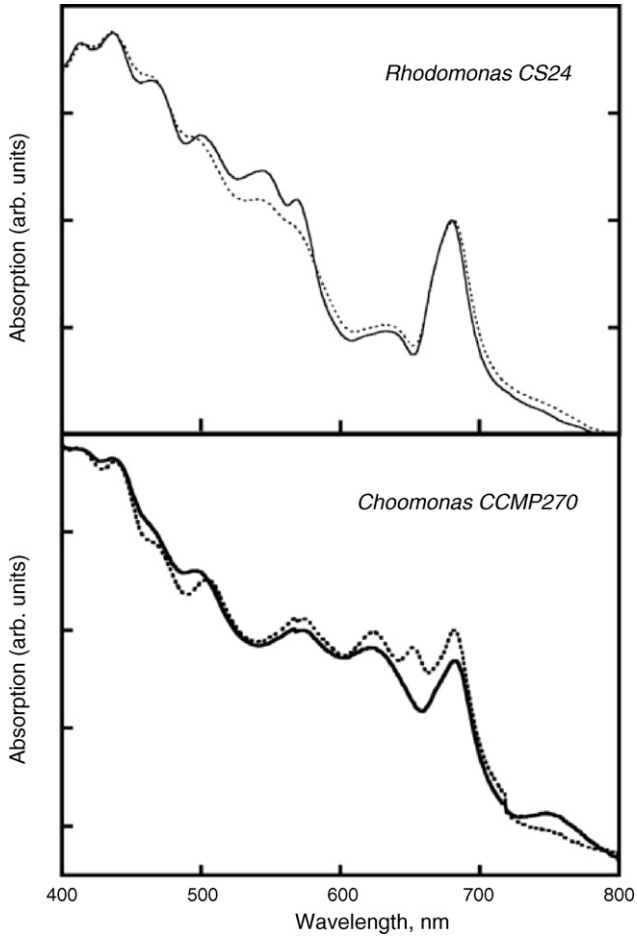

Fig. 10. Room temperature (dotted) and 77 K (solid) absorption spectra of *Rhodomonas CS24* and *Chroomonas CCMP270* algal cells.

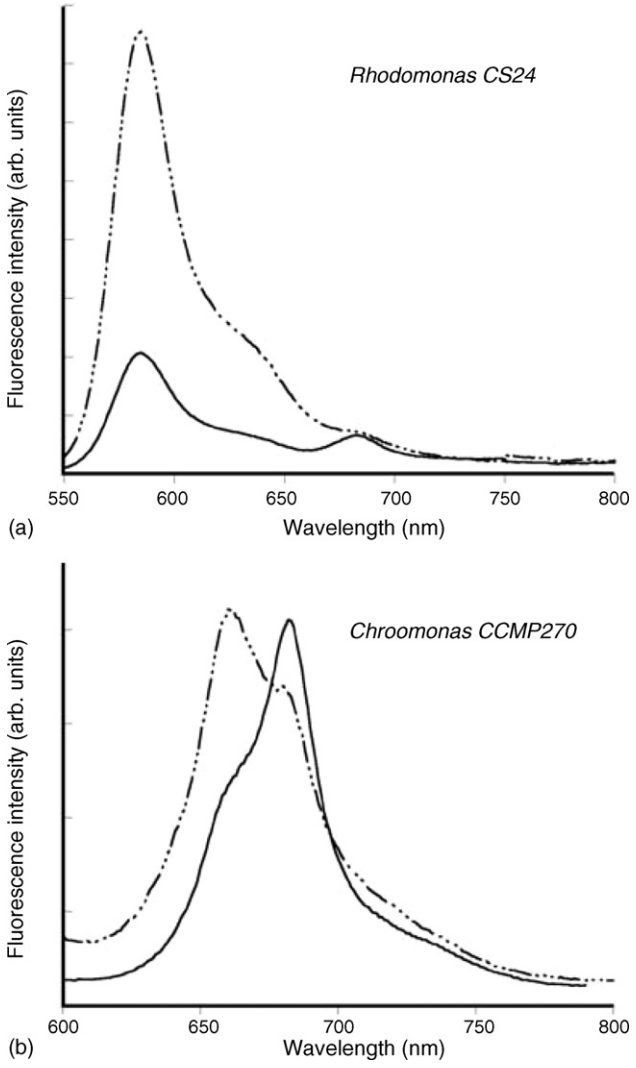

Fig. 11. (a) Emission spectra of intact *Rhodomonas CS24* cells at room temperature at two selected excitation wavelengths: 400 nm (solid line) and 500 nm (broken line). The peaks correspond to PE545 emission (585 nm) and Chl *a* (684 nm). (b) Emission spectra of *Chroomonas CCMP270* at room temperature at two excitation wavelengths: 400 nm (solid line) and 520 nm (broken line). The peaks correspond to PC645 emission (660 nm) and Chl *a* (684 nm).

Significant PE545 emission is evident, suggesting that energy transfer from PE545 to the membrane-bound Chls is not 100% efficient. At room temperature, the Chl *a* emission maximum is at 686 nm. At 77 K, an emission maximum is evident at 701 nm, with a shoulder at 684 nm. The former emission band is clearly red-shifted with respect to the expected PS II emission bands at 685 and 695 nm [110].

The characteristic PS I emission bands (77 K) at 715, 725 and 730 nm (different cryptophytes [13]) or 735 nm (green plants) were not observed in our measurements. It is therefore suggested that the 701 nm fluorescence has a contribution from PS I emission. Furthermore, this means that PS I of *Rhodomonas CS24* may not contain 'red' chlorophylls. Such 'red' chlorophylls are known to be associated with the core and/or peripheral antenna of PS I of higher plants and cyanbacteria. They absorb at longer wavelengths than the primary electron donor P700, though their precise function has not been decided [111].

When excitation was tuned in the range 400–480 nm, a Chl *c2* emission peak was observed at 640 nm. The appearance of this emission is remarkable, because in isolated Chl *a*/*c2* complexes, the Chl *c2* delivers its excitation energy efficiently to Chl *a* [50] and Chl *c2* emission should not be observed. Perhaps a small part of Chl *c2* exists as a free pigment in the membrane. From the steady-state data it cannot be determined whether PE545 transfers excitation directly to Chl *a*, or whether Chl *c2* plays an intermediate role in the energy transfer scheme.

The fluorescence excitation spectra of the intact algae detected at 686 and 696 nm, respectively, recording PS II and a mixture of PS I/PS II emission, show clearly the energy transfer from PE545 to the photosynthetic reaction centers. However, owing to significant overlap between the emission bands of PS I and PS II, the fluorescence excitation spectra cannot conclusively reveal whether the excitation energy is preferentially transferred to PS II or PS I. The fluorescence intensities as a function of both wavelength and time for isolated PE545 compared to intact algae are shown in Fig. 12. The quenching of PE545 emission by the chlorophylls is obvious from the fast ($\ll$2.5 ns) PE545 emission decay at the blue edge of the image and corresponding fast rise time of the 685 nm emission band.

By fitting a necessarily complicated kinetic model to the fluorescence data, the timescales by which the energy is transferred from PE545 to the Chls in the membrane could be obtained. That modeling is described in detail in Ref. [48]. Our conclusions are summarized here. Initially, PE545, PS I and PS II were photo-excited at 562 nm in a ratio estimated to be 96:4:2 from the kinetic analysis, in accordance with the absorption spectrum. This excitation ratio highlights how effective PE545 is in absorbing light in the green spectral region relative to the Chls. PE545 fluorescence decay times of 17, 58, 113 and 2500 ps were resolved. The kinetic model of the subsequent dynamics allowed for energy transfer from PE545 to both PS I and PS II

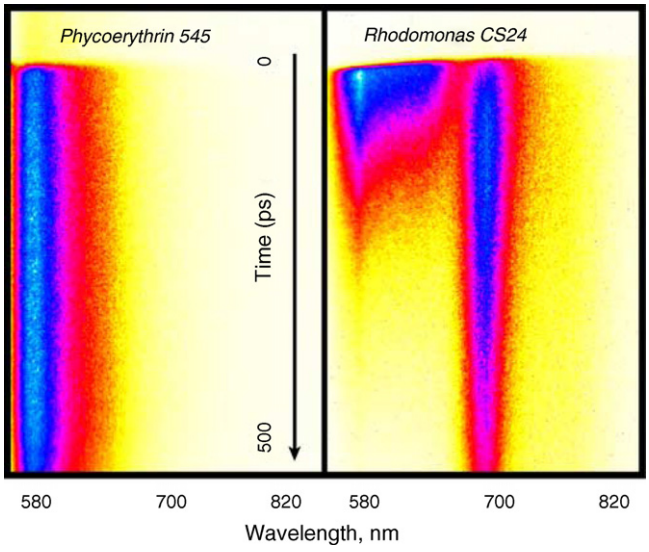

Fig. 12. Raw data images from the streak camera experiment of the fluorescence from PE545 and the intact *Rhodomonas CS24* algae adapted from Ref. [48]. These data were recorded under magic angle with a 500 ps time delay.

in a fixed ratio. It was estimated that PS II received 45% of the energy flowing out of PE545, whereas the other 55% migrated to PS I.

The PS II core has a large mass of protein in the lumen that does not contain pigments (extrinsic proteins involved in water oxidation), which makes direct energy transfer from PE545 to the PS II core difficult. However, the PS II core probably binds peripheral Chl *alc2* antenna complexes, making PE545 → Chl *a*/*c2* → PS II core energy transfer possible, as illustrated in the model proposed by Mimuro et al. [58]. PS I has little protein mass in the lumen, making direct PE545 to PS I core energy transfer more facile. This is being reflected by the faster transfer rate constants of energy transfer from PE545 to PS I.

In the experiments on isolated PE545, it had been found that excitation energy migrates to the DBV bilins within just a few ps [79]. Thus the longer energy transfer time scales of 17, 58 and 113 ps obtained from analysis of the intact algae data are ascribed to DBV bilin to Chl energy transfer. Such rapid energy transfer is necessary to achieve a high light-harvesting efficiency. Indeed, the data analysis suggest that only two percent of PE545 excitation energy remains unquenched during its fluorescence lifetime of 2.5 ns, illustrating the near perfect energy transfer efficiency from PE545 to the Chls in the membrane.

The dimensions of the lumen compared to PE545 imply an angular and spatial distribution of PE545 around the periphery of the photosystems in the membrane (Fig. 2). Together with the relative orientation of donor DBV and acceptor Chl, this leads to a distribution of PE545 to Chl energy transfer time scales. A model whereby excitation energy equilibrates in PE545 (i.e. to the α19-A DBV) prior to sensitization of membrane-bund chlorophyll cannot account for the experimental results; on average the predicted energy transfer time is too slow. It is concluded that energy transfer must occur from both DBV bilins to membrane-bound chlorophyll, in competition with energy transfer from α19-B to a α19-A, in order to overcome the large distance distribution of energy rates predicted by assuming only one DBV could be an energy transfer donor. The interesting implication of that conclusion is that the antenna functions more effectively in the organism than was indicated by experiments on the isolated PE545 antenna complex.

4.2. *Chroomonas CCMP270*

The absorption spectra of *Chroomonas CCMP270* algae at room temperature and 77 K are shown in Fig. 10. In comparison to the absorption spectrum of *Rhodomonas CS24*, the blue-shift of the phycobiliprotein antenna complex is clearly evident. The assignment of the spectral positions of the pigments in the two cryptophyte organisms was, besides PE545 and PC645, identical, and were analyzed using the second derivative spectra of the 77 K trace. The most dominant Chl *a* peak is at 682 nm, with some satellite bands at 671, 668 and 610 nm, and the Soret band at 443 nm. Most Chl *c2* absorption features are hidden by the absorption peaks of PC645 at 585, 522 and 645 nm, respectively, except for the Chl *c2* Soret band, seen at 471 nm. The carotenoids, mainly alloxanthin, absorb at around 425 and 570 nm.

The emission spectra at room temperature are shown in Fig. 11. In the figure, PC645 emission is at 660 nm and Chl *a* emission at 684 nm. Owing to the better spectral overlap, the efficiency of energy transfer of excitation from PC645 to the membrane Chls was found to be even better than the 98% efficient energy transfer of PE545 to the membrane Chls. A noticeable difference between the room temperature emission spectra of the *Rhodomonas* and *Chroomonas* organisms is that in the former, the intensity of Chl *a* emission does not vary much at differing excitation wavelengths, whereas in the latter, the excitation wavelength determines greatly the intensity of the Chl *a* emission.

5. Conclusions

We have described a comprehensive study of the dynamics of light-harvesting by the phycobiliproteins phycoerythrin 545 (PE545) and phycocyanin 645 (PC645); antenna complexes in cryptophyte algae. Using a combination of steady-state and ultrafast spectroscopies in conjunction with global analyses and calculations of excited states, electronic coupling and energy transfer rates, a detailed picture of function was revealed. Energy transfer and trapping dynamics occurring on time scales from tens of femtoseconds to tens of picoseconds were associated with the structural model as well as a spectral model. Relating spectral bands to structural models is a great challenge since subtle interactions between the environment and the chromophores can tune electronic absorption features. PE545 and PC645 are obviously rather different, considering their absorption spectra. Nonetheless, it seems that the basic picture of ultrafast excitation energy funneling to the pair of peripheral α19 bilins (DBV or MBV), followed by slower energy transfer to just one of those chromophores is similar for each antenna complex. Taking the study a step further, time-resolved fluorescence experiments on intact *Rhodomonas CS24* cells allowed us to elucidate a model that describes how excitation energy is transferred to the membrane-associated Chls of PS I and PS II. Considering the organization of the thylakoid membrane, which is outlined in Fig. 2, we suggested that the Chl *a*/*c2* complex mediates the PE545 to PS II energy transfer, while PS I is sensitized directly. Importantly, it was discovered that energy transfer from the phycobilin to the membrane Chls does not occur from the emitting bilin only – a conclusion that would reasonably be drawn from studies of isolated antenna complexes – rather, both peripheral α-subunit bilins mediate sensitization of Chl. It was thus illustrated that spectroscopic experiments on isolated components cannot necessarily predict a precise dynamical picture of how these proteins function in the intact species.

Acknowledgements

The Natural Sciences and Engineering Council of Canada are acknowledged for financial support. We gratefully acknowledge our co-workers and colleagues: Delmar Larsen, Ivo van Stokkum, Chantal van der Weij-de Wit, Jan Dekker, Rienk van Grondelle (Vrije Universiteit, Amsterdam) and Brent Krueger (Hope College). GDS thanks the Alfred P. Sloan foundation.

References

[1] D.J. Des Marais, Science 289 (2000) 1703–1705.
[2] J.W. Schopf (Ed.), Major Events in the History of Life, Jones and Bartlett, 1992.
[3] J. Xiong, W.M. Fischer, K. Inoue, M. Nakahara, C.E. Bauer, Science 289 (2000) 1724–1730.
[4] A.N. Glazer, Biochim. Biophys. Acta 768 (1984) 29–51.
[5] J.F. Kasting, J.L. Siefert, Science 296 (2002) 1066–1068.
[6] H. Gest, Photosynth. Res. 73 (2002) 7–10.
[7] B.L. Clay, P. Kugrens, R.E. Lee, Bot. J. Linnean Soc. 131 (1999) 131–151.
[8] T.I. Bergmann, PhD Thesis, Rutgers, The State University of New Jersey, 2004.
[9] G.I. McFadden, J. Phycol. 37 (2001) 951–959.
[10] L. Spear-Bernstein, K.R. Miller, J. Phycol. 25 (1989) 412–419.
[11] R. MacColl, D. Guard-Friar, Phycobiliproteins, CRC Press, Boca Raton, FL, 1987.
[12] E. Gantt, in: M. Levandowsky, S.H. Hutner (Eds.), Biochemistry and Physiology of Protazoa, vol. 1, Academic Press, New York, 1979.
[13] D. Bruce, J. Biggins, T. Steiner, M. Thewalt, Photochem. Photobiol. 44 (1986) 519–525.
[14] W.A. Sidler, in: D.A. Bryant (Ed.), The Molecular Biology of Cyanobacteria, Advances in Photosynthesis, vol. 1, Kluwer Academic Publishers, Dordrecht, The Netherlands, 1994.
[15] L. Cheng, L. Jiang, Chin. Chem. Lett. 2 (1991) 589–592.
[16] S.E. Braslavsky, A.R. Holzwarth, K. Schaffner, Angew. Chem. Int. Ed. Engl. 22 (1983) 656–674.
[17] R. MacColl, I. Lam, C.Y. Choi, J. Kim, J. Biol. Chem. 269 (1994) 25465–25469.
[18] R. MacColl, L.E. Eisele, M. Dhar, J.P. Ecuyer, S. Hopkins, J. Marrone, R. Barnard, H. Malak, A.J. Lewitus, Biochemistry 38 (1999) 4097–4105.
[19] D.M. Jonas, M.J. Lang, Y. Nagasawa, T. Joo, G.R. Fleming, J. Phys. Chem. 100 (1996) 12660–12673.
[20] H. Sumi, J. Phys. Chem. B 103 (1999) 252–260.
[21] G.D. Scholes, X.J. Jordanides, G.R. Fleming, J. Phys. Chem. B 105 (2001) 1640–1651.
[22] D.C. Arnett, C.C. Moser, P.L. Dutton, N.F. Scherer, J. Phys. Chem. B 103 (1999) 2014–2032.
[23] H. Kikuchi, H. Wako, K. Yura, M. Go, M. Mimuro, Biophys. J. 79 (2000) 1587–1600.
[24] H. Kikuchi, T. Sugimoto, M. Mimuro, Chem. Phys. Lett. 274 (1997) 460–465.
[25] H. Scheer, Proceedings of the 13th International Congress of Photosynthesis, Book of Abstracts, Montreal, 2004.
[26] T. Förster, Ann. Phys. 2 (1948) 55–75.
[27] B.W. Van der Meer, G. Coker, S.-Y.S. Chen, Resonance Energy Transfer: Theory and Data, VCH, New York, 1994.
[28] H. van Amerongen, L. Valkunas, R. van Grondelle, Photosynthetic Excitons, World Scientific, Singapore, 2000.
[29] R. van Grondelle, Biochim. Biophys. Acta 811 (1985) 147–195.
[30] V. Sundström, T. Pullerits, J. Phys. Chem. B 103 (1999) 2327–2346.
[31] G.R. Fleming, R. van Grondelle, Curr. Opin. Struct. Biol. 7 (5) (1997) 738–748.
[32] G.D. Scholes, Annu. Rev. Phys. Chem. 54 (2003) 57–87.
[33] G.D. Scholes, G.R. Fleming, Adv. Chem. Phys. 132 (2005) 57–130.
[34] T. Förster, in: O. Sinanoglu (Ed.), Modern Quantum Chemistry, vol. III, Academic Press, New York, USA, 1965.
[35] V.M. Agranovich, M.D. Galanin, in: V.M. Agranovich, A. Maradudin (Eds.), Modern Problems in Condensed Matter Science, vol. 3, North-Holland, Amsterdam, 1982, p. 171.
[36] S. Speiser, Chem. Rev. 96 (1996) 1953–1976.
[37] R.D. Harcourt, G.D. Scholes, K.P. Ghiggino, J. Chem. Phys. 101 (1994) 10521–10525.
[38] G.D. Scholes, R.D. Harcourt, K.P. Ghiggino, J. Chem. Phys. 102 (1995) 9574–9581.
[39] G.D. Scholes, R.D. Harcourt, J. Chem. Phys. 104 (1996) 5054–5061.
[40] H. Wiesenhofer, D. Beljonne, G.D. Scholes, E. Hennebicq, J.-L. Brédas, E. Zojer, Adv. Funct. Mater. 15 (2004) 155–160.
[41] R. van Grondelle, V.I. Novoderezhkin, Phys. Chem. Chem. Phys. 8 (7) (2006) 793–807.
[42] V.I. Novoderezhkin, M.A. Palacios, H. van Amerongen, R. van Grondelle, J. Phys. Chem. B 108 (2004) 10363–10375.
[43] R. van Grondelle, V.I. Novoderezhkin, Biochemistry 40 (2001) 15057–15068.
[44] M. Yang, A. Damjanovic, H.M. Vaswani, G.R. Fleming, Biophys. J. 85 (2003) 140–158.
[45] M. Yang, G.R. Fleming, Chem. Phys. 275 (2002) 355–372.
[46] S.J. Jang, M.D. Newton, R.J. Silbey, Phys. Rev. Lett. 92 (2004) 218301.
[47] G.R. Fleming, G.D. Scholes, Nature 431 (2004) 256–257.
[48] C. van der Weij-de Wit, A.B. Doust, J.P. Dekker, I.H.M. van Stokkum, K.E. Wilk, P.M.G. Curmi, R. van Grondelle, G.D. Scholes, submitted for publication.
[49] L. Bathke, E. Rhiel, W.E. Krumbein, J. Marquardt, Plant Biol. 1 (1999) 516–523.
[50] K. Ingram, R.G. Hiller, Biochim. Biophys. Acta 722 (1983) 310–319.
[51] R.G. Hiller, C.D. Scaramuzzi, J. Breton, Biochim. Biophys. Acta 1102 (1992) 360–364.
[52] D.R.A. Hill, K.S. Rowan, Phycologia 28 (4) (1989) 455–463.
[53] C. Lichtlé, J.C. Duval, Y. Lemoine, Biochim. Biophys. Acta 894 (1987) 76–90.
[54] C.M. Toole, F.C.T. Allnutt, in: A.W.D. Larkum, S.E. Douglas, J.A. Raven (Eds.), Algal Phycobiliproteins in Photosynthesis in Algae, Kluwer Academic Publishers, Dordrecht, The Netherlands, 2003, p. 305.
[55] J.P. Dekker, E.J. Boekema, Biochim. Biophys. Acta 1706 (2005) 12–39.
[56] C. Lichtlé, J.C. Duval, N. Hauswirth, A. Spilara, Photobiochem. Photobiophys. 11 (3) (1986) 159–171.
[57] C. Lichtlé, H. Jupin, J. Duval, Biochim. Biophys. Acta 591 (1980) 104–112.
[58] M. Mimuro, N. Tamai, A. Murakami, M. Watanabe, M. Erata, M. Watanabe, M. Tokutomi, I. Yamazaki, Phycol. Res. 46 (1998) 155–164.
[59] A.B. Doust, C.N.J. Marai, S.J. Harrop, K.E. Wilk, P.M.G. Curmi, G.D. Scholes, J. Mol. Biol. 344 (1) (2004) 135–153.
[60] K.E. Wilk, S.J. Harrop, L. Jankova, D. Edler, G. Keenan, F. Sharpies, R.G. Hiller, P.M.G. Curmi, Proc. Natl. Acad. Sci. U.S.A. 96 (1999) 8901–8906.
[61] O. Nanba, K. Satoh, Proc. Natl. Acad. Sci. U.S.A. 84 (1987) 109–112.
[62] R. MacColl, L.E. Eisele, J. Marrone, Biochim. Biophys. Acta 1412 (1999) 230–239.
[63] R. MacColl, H. Malak, J. Cipollo, B. Label, G. Ricci, D. MacColl, L. Eisele, J. Biol. Chem. 270 (1995) 27555–27561.
[64] S.E. Boiadjiev, D.A. Lightner, Tetrahedron: Asymmetry 10 (1999) 607–655.
[65] E. Charney, The Molecular Basis of Optical Activity: Optical Rotatory Dispersion and Circular Dichroism, John Wiley & Sons, New York, 1979.
[66] R. Alison, B. Nordén, Circular Dichroism & Linear Dichroism, Oxford University Press, Oxford, UK, 1997.
[67] C.C. Gradinaru, I.H.M. van Stokkum, A.A. Pascal, R. van Grondelle, H. van Amerongen, J. Phys. Chem. B 104 (2000) 9330–9342.
[68] M.D. Fayer, Annu. Rev. Phys. Chem. 33 (1982) 63–87.
[69] D.S. Larsen, K. Ohta, Q.-H. Xu, M. Cyrier, G.R. Fleming, J. Chem. Phys. 114 (18) (2001) 8008–8019.
[70] T. Joo, Y. Jia, J.-Y. Yu, M.J. Lang, G.R. Fleming, J. Chem. Phys. 104 (1996) 6089–6108.
[71] I.H.M. van Stokkum, K. Müllen, Notes and data analysis with TIM, 2004. This document is available in HTML, pdf and ps version from: http://www.nat.vu.nl/~kate/TIM.
[72] A.R. Holzwarth, in: J. Amesz, A.J. Hoff (Eds.), Biophysical Technique in Photosynthesis, Kluwer Academic Publishers, Dordrecht, The Netherlands, 1996.
[73] I.H.M. van Stokkum, D.S. Larsen, R. van Grondelle, Biochim. Biophys. Acta 1657 (2004), 82–104 and 1658, 262 (erratum).
[74] B.J. Homoelle, M.D. Edington, W.M. Diffey, W.F. Beck, J. Phys. Chem. B 102 (1998) 3044–3052.
[75] H. Barkhuijsen, R. Debeer, D. Ormondt, J. Magn. Reson. 73 (3) (1987) 553–557.

[76] J.M. Salverda, M. Vengris, B.P. Krueger, G.D. Scholes, A.R. Czarnoleski, V. Novoderezhkin, H. van Amerongen, R. van Grondelle, Biophys. J. 84 (2003) 450–465.
[77] L.D. Book, A.E. Ostafin, N. Ponomarenko, J.R. Norris, N.F. Scherer, J. Phys. Chem. B 104 (2000) 8295–8307.
[78] V.I. Prokhorenko, A.R. Holzwarth, F.R. Nowak, T.J. Aartsma, J. Phys. Chem. B 106 (2002) 9923–9933.
[79] A.B. Doust, I.H.M. van Stokkum, D.S. Larsen, K.E. Wilk, P.M.G. Curmi, R. van Grondelle, G.D. Scholes, J. Phys. Chem. B 109 (2005) 14219–14226.
[80] M.J. Frisch, G.W. Trucks, H.B. Schlegel, G.E. Scuseria, M.A. Robb, et al., Gaussian 03, Revision C.02, Gaussian, Inc., Wallingford, CT, 2004.
[81] J.B. Foresman, A. Frisch, Exploring Chemistry with Electronic Structure Methods: A Guide to Using Gaussian, 2nd ed., Gaussian, 1996.
[82] J.B. Foresman, M. Head-Gordon, J.A. Pople, M.J. Frisch, J. Phys. Chem. 96 (1992) 135–149.
[83] B.P. Krueger, G.D. Scholes, G.R. Fleming, J. Phys. Chem. B 102 (1998) 5378–5386.
[84] G.D. Scholes, I.R. Gould, R.J. Cogdell, G.R. Fleming, J. Phys. Chem. B 103 (1999) 2453–2553.
[85] R. MacColl, D.S. Berns, Photochem. Photobiol. 27 (1978) 343–349.
[86] G.D. Scholes, G.R. Fleming, J. Phys. Chem. B 104 (2000) 1854–1868.
[87] E. Hennebicq, G. Pourtois, G.D. Scholes, L.M. Herz, D.M. Russell, C. Silva, S. Setayesh, K. Müllen, J.L. Brédas, D. Beljonne, J. Am. Chem. Soc. 127 (2005) 4744–4762.
[88] T. Meier, V. Chernyak, S. Mukamel, J. Chem. Phys. 107 (1998) 8759–8780.
[89] H. Fidder, J. Knoester, D.A. Wiersma, J. Chem. Phys. 95 (1991) 7880–7890.
[90] Y.J. Yan, S. Mukamel, J. Chem. Phys. 85 (1986) 5908–5923.
[91] B. Li, A.E. Johnson, S. Mukamel, A.B. Myers, J. Am. Chem. Soc. 166 (1994) 11039–11047.
[92] M.D. Edington, R.E. Riter, W.F. Beck, J. Phys. Chem. 100 (1996) 14206–14217.
[93] A.N. Glazer, C.S. Hixson, J. Biol. Chem. 250 (14) (1975) 5487–5495.
[94] T. Jiang, J. Zhang, W. Chang, D. Liang, Biophys. J. 81 (2001) 1171–1179.
[95] M.P. Debreczeny, K. Sauer, J. Zhou, D.A. Bryant, J. Phys. Chem. 99 (1995) 8420–8431.
[96] K. Csatorday, D. Guard-Friar, R. MacColl, D.S. Berns, Photochem. Photobiol. 47 (1988) 285–291.
[97] R. MacColl, E.C. Williams, L.E. Eisele, P. McNaughton, Biochemistry 33 (1994) 6418–6423.
[98] G.D. Goodno, R.J.D. Miller, J. Phys. Chem. A 103 (1999) 10619–10629.
[99] M. Khalil, N. Demirdoven, O. Golonzka, C.J. Fecko, A. Tokmakoff, J. Phys. Chem. A 104 (2000) 5711–5715.
[100] Q.-H. Xu, Y.Z. Ma, G.R. Fleming, Chem. Phys. Lett. 338 (2001) 254–262.
[101] Q.-H. Xu, Y.Z. Ma, I.V. Stiopkin, G.R. Fleming, J. Chem. Phys. 116 (21) (2002) 9333–9340.
[102] C. Scharnagl, S. Schneider, J. Photochem. Photobiol. B: Biol. 3 (1989) 603–614.
[103] C. Scharnagl, S. Schneider, J. Photochem. Photobiol. B: Biol. 8 (1991) 129–157.
[104] A.R. Holzwarth, J. Wendler, W. Wehrmeyer, Biochim. Biophys. Acta 724 (1983) 388–395.
[105] B. Gobets. PhD Thesis, Vrije Universiteit, Amsterdam, 2002.
[106] T. Ito, M. Hiramatsu, M. Hosoda, Y. Tsuchiya, Rev. Sci. Instrum. 62 (1991) 1415–1419.
[107] T.M. Nordlund, in: J.R. Lakowicz (Ed.), Topics in Fluorescence Spectroscopy, Plenum Press, New York, 1991.
[108] G. Harnischfeger, B. Herold, Berichte Der Deutschen Botanischen Gesellschaft 94 (1981) 65–73.
[109] J. Stoń, A.J. Kosakowska, Appl. Phycol. 14 (2002) 205–210.
[110] E.G. Andrizhiyevskaya, A. Chojnicka, J.A. Bautista, B.A. Diner, R. van Grondelle, J.P. Dekker, Photosynth. Res. 84 (2005) 173–180.
[111] B. Gobets, R. van Grondelle, Biochim. Biophys. Acta 1507 (2001) 80–99.